Toroidal Symmetry of the Geodesic Acoustic Mode Zonal Flow in a Tokamak Plasma

K. J. Zhao,[1] T. Lan,[2] J. Q. Dong,[1] L. W. Yan,[1] W. Y. Hong,[1] C. X. Yu,[2] A. D. Liu,[2] J. Qian,[1] J. Cheng,[1] D. L. Yu,[1] Q. W. Yang,[1] X. T. Ding,[1] Y. Liu,[1] and C. H. Pan[1]

[1]*Southwestern Institute of Physics, P.O. Box 432, Chengdu, China*

[2]*Department of Modern Physics, University of Science and Technology of China, Hefei, China*

(Received 24 February 2006; revised manuscript received 28 April 2006; published 27 June 2006)

The toroidal symmetry of the geodesic acoustic mode (GAM) zonal flows is identified with toroidally distributed three step Langmuir probes at the edge of the HuanLiuqi-2A (commonly referred to as HL-2A) tokamak plasmas for the first time. High coherence of both the GAM and the ambient turbulence for the toroidally displaced measurements along a magnetic field line is observed, in contrast with the high coherence of the GAM but low coherence of the ambient turbulence when the toroidally displaced measurements are not along the same field line. The radial and poloidal features of the flows are also simultaneously determined. The nonlinear three wave coupling between the high frequency turbulent fluctuations and the flows is demonstrated to be a plausible formation mechanism of the flows.

DOI: 10.1103/PhysRevLett.96.255004 PACS numbers: 52.35.Ra, 52.25.Fi, 52.35.Mw, 52.55.Fa

Zonal flows are universal phenomena in nature and have attracted intense interest in the magnetic fusion plasma physics community in recent years [1–21]. The active studies in this field are aimed at an understanding of nonlinear physics processes responsible for coherent structure formation and for anomalous transport in plasmas.

The transport anomaly is attributed to small scale fluctuations. Theoretical studies have found that, besides inducing turbulent transport, the fluctuations can create coherent zonal flows that, in turn, regulate the former [2]. The mechanism for coherent flow generation and the flow-turbulence interaction dynamics are among important basic scientific topics in modern physics. Two kinds of zonal flows have been identified in magnetically confined toroidal plasmas, i.e., the near zero low frequency zonal flow (LFZF) [6–9] and the geodesic acoustic mode zonal flow (GAMZF) [10–21]. In this Letter, the GAM flows will be focused on only. Theory and simulations predict that the GAMZFs share the major features: (1) radially localized, (2) axisymmetric ($k_\phi = 0$, $n = 0$) and (3) poloidally symmetric ($k_\theta = 0$, $m = 0$) potential and asymmetric ($m = 1$) density perturbations, (4) the flux-surface average mainly in the poloidal direction, and (5) frequency of $f_{\mathrm{GAM}}^{\mathrm{th}} \sim (\sqrt{(T_e + T_i)/M_i}/2\pi R)(1 + 1/2q^2)$ and collisionless and collisional damping rates of $\gamma_L \sim \omega \exp(-\alpha q^2)$ and $\gamma_c \sim 4\nu_{\mathrm{ii}}/7$ [3–5]. Here k_ϕ and k_θ are toroidal and poloidal components of a wave vector, respectively, n and m are corresponding mode numbers, R is the major radius of the plasma torus, q is a safety factor, ν_{ii} is the ion-ion collision frequency, and α is a factor of order unity.

GAMZF studies have been reported from a few devices. The structure in a poloidal cross section and characteristics of the flows were studied [12–15] with beam emission spectroscopy at the plasma edge in the DIII-D tokamak. Similar experiments were conducted with a heavy ion beam probe (HIBP) in the core of the JIPP-TIIU tokamak plasmas [16]. Two types of coherent modes ($f \sim 1$ and $\sim$12 kHz) with small poloidal wave numbers were measured with a plane Langmuir probe (LP) array in JFT-2M [17]. The radial and poloidal features of the GAM oscillations were investigated in ASDEX upgrade using Doppler reflectometry [18] and in JFT-2M with a HIBP [19]. The oscillations were also detected with correlation reflectometry and LP in the T-10 device [20,21].

Observation of zonal flow structure in the toroidal direction was performed on the compact helical system [6]. Toroidal structure of ZFs has not been reported from tokamak devices. In particular, simultaneous determination of poloidal and toroidal features of LFZFs as well as GAMZFs has never been conducted.

The toroidal symmetry ($n \simeq 0$) of the GAMZFs has been identified with three step Langmuir probe (TSLP) arrays [see Fig. 1(a)] at the edge of the HuanLiuqi-2A (HL-2A) tokamak plasmas for the first time, recently. The coherences of both the GAMZFs and the ambient turbulence (AT) for the toroidally displaced measurements along and not along a magnetic field line are estimated and compared. Three-dimensional (3D) features of the electric field are analyzed and presented in this Letter.

The major and minor radii of the HL-2A tokamak are $R = 1.65$ m and $a = 0.4$ m [22], respectively. The experiments presented here were conducted in Ohmic heated hydrogen plasmas of a circular cross section. The parameters specially set for these experiments (shots 4044 and 4206) are toroidal magnetic field $B_t = 2.3$–2.4 T, the discharge duration $t_d = 2$ s, besides those summarized in Table I, where given, from the left to the right, are the shot number, the radial position of the LPs r/a, the plasma current I_p, the line averaged electron density $\bar{n}_e$, the boundary safety factor q_a, the ion Larmor radius ρ_i, and the electron temperature at the LP position T_e.

The fluctuations of a floating electrostatic potential were measured with three arrays of TSLPs displaced toroidally

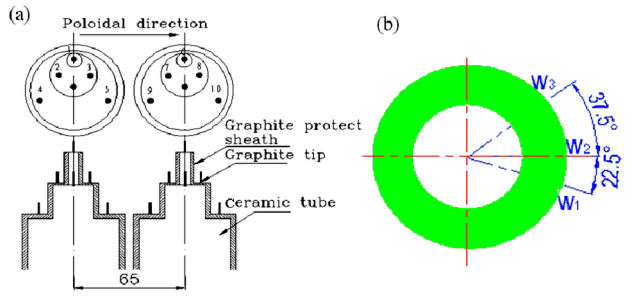

FIG. 1 (color online). (a) Structure and (b) layout of the three step Langmuir probes.

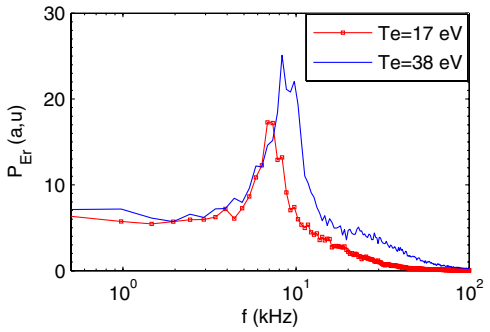

FIG. 2 (color online). Representative autopower spectra of the fluctuating E_r.

and poloidally. Each TSLP array is composed of 5 probes possessing 4 and 7 (at the bottom step)/4.5 (at the middle step) mm separations in the radial and poloidal directions [see Fig. 1(a)]. Two of them forming a magnetomotive 10 probe set were placed in the same poloidal cross section with a separation of 65 mm in the poloidal direction [W1 in Fig. 1(b)], while the third array of electromotive 6 probes (numbered 11–16) was located 800 mm away in the toroidal direction [W2 in Fig. 1(b)]. The probe set and the third array were both mounted at the outside middle plane of the tokamak up-down symmetrically. There was a fourth array of fast reciprocating 6 probes which measures electron temperature and density profiles in the edge region [W3 in Fig. 1(b)]. The length and diameter of each probe tip are 2 and 1.5 mm, respectively.

The sampling rate of the LP signals is 1 MHz corresponding to the Nyquist frequency $f_N = 500$ kHz. No significant signals were detected when the LPs were placed outside the $r/a = 1$ surface. The collision frequency and the safety factor at the LP locations are estimated as $\nu_{ii} \sim (1.5\text{–}3.0) \times 10^4/\mathrm{s}$ and $q((r/a) = 0.93) \simeq 0.88 q_a$.

The principles and schemes for the data analysis are well documented and will not be repeated [23,24]. Two hundred sets of 2^{11} data records each were used and the frequency resolution was 0.48 kHz in the following analysis unless otherwise stated.

The representative autopower spectra of the fluctuating E_r are given in Fig. 2. The frequencies at the centers of the peaks in the spectra, f_{GAM}, are given in Table I. The calculated GAM frequencies with the above formula are $f^{\mathrm{th}}_{\mathrm{GAM}} = 5.51$ and 8.23 kHz, for $T_e = 17$ and 38 eV, respectively, assuming $T_e = T_i$. The scaling $f_{\mathrm{GAM}} \simeq 1.18 f^{\mathrm{th}}_{\mathrm{GAM}}$ holds for the results, indicating that the frequencies of the centers are in good agreement with GAM theory prediction. The lifetime of the GAMZF may be estimated as 200–300 μs from the widths of 3–5 kHz of the peaks. This is 25 times the decorrelation time $\tau_d \sim 10$ μs of the AT when ZFs are present. Spatially, the estimated poloidal correlation length for the ATs is $l_\theta \sim 2$ cm, which is much shorter than the corresponding scale length of the GAMZFs described below. On the other hand, the radial correlation length of the ATs is estimated to be $l_r \sim 1$ cm, which is comparable with the radial scale length of the GAMZFs. The spatial characteristics of the GAM frequency fluctuations only will be described and discussed more in detail in this Letter, while ATs are left for future works. In addition, while the focus of this Letter is on GAMs, an attempt to measure the LFZF was made as well. The LFZFs were absent in these two discharges.

Shown in Fig. 3(a) are the coherency spectra of $E_{r1} = (\phi_{f1} - (\phi_{f2} + \phi_{f3})/2)/\delta r$ and $E_{r2} = (\phi_{f6} - (\phi_{f7} + \phi_{f8})/2)/\delta r$ for the two shots. Here δr is the radial separation of the probe tips at neighboring steps. The coherencies of 0.6 and 0.79 in the GAMZF frequency region clearly demonstrate the strong correlation of the fluctuations over the $d_\theta = 65$ mm distance, which is much longer than the correlation length estimated above for the ATs in the poloidal direction. The dashed line indicates the uncertainty level in the coherency spectra.

The phase differences $\Delta\phi_\theta$ between E_{r1} and E_{r2} are given in Fig. 3(b). On average over the width of half maximum, the poloidal wave vectors of the GAMZFs are $k_\theta = -0.02 \pm 0.01$ and -0.05 ± 0.03 cm^{-1}, respectively. The discrepancy of the estimated mode numbers $m \leq 1$ and $m < 2$ will be discussed later. The poloidal wave vector k_θ versus frequency f is also estimated from ϕ_{f2} and ϕ_{f3} and given in Fig. 3(c). Here the general dispersion relations, straight lines without offsets, for the ATs (due to the $d_\theta = 4.5$ mm short distance between the two probe tips) and the deviations from it in the GAM frequency region are clearly shown. The ATs propagate in the electron diamagnetic drift direction.

TABLE I. Parameters for the GAMZF experiments.

Shot number	r/a	Ip (kA)	$\bar{n}_e$ (10^{13} cm^3)	q_a	ρ_i (10^{-2} cm)	Te (eV)	f_{GAM} (kHz)
4206	0.92	300	2.5	3.5	1.8	17	6.8
4044	0.93	200	2	5.3	2.7	38	9.3

The spatial characteristics of the radial electric field in the toroidal direction are described in Fig. 4. First, given here are (a) the coherency spectra of E_{r1} and $E_{r3} = (\phi_{f11} - (\phi_{f12} + \phi_{f13})/2)/\delta r$ and (b) phase differences $\Delta\phi_t$ between E_{r1} and E_{r3}. Here the dashed lines do the same as that in Fig. 2. The coherent structure of the GAM frequency oscillations over the $d_t = 800$ mm distance in the toroidal direction is clearly illustrated by the coherencies of 0.9 and 0.96 for the two shots. The sharp decreases of the phase shift in the GAM frequency region noticeably distinguish the GAMZFs from the ATs. The calculated toroidal wave vectors in the GAMZF frequency region are $k_\phi \simeq (0.02 \pm 0.07) \times 10^{-2}$ and $(0.22 \pm 0.04) \times 10^{-2}$ cm^{-1} from this set of data. The corresponding toroidal mode numbers are $n = 0.0 \pm 0.1 \simeq 0$ and $0.33 \pm 0.07 \simeq 0$. We note that the coherencies in the AT frequency region ($f > 20$ kHz) are lower than that of the GAMZFs but not significantly low (especially for shot 4044). In addition, the phase shifts in Fig. 4(b) exhibit clear linear dispersion relations in that region. These indicate that the correlation of the ATs over the 800 mm distance in the direction from probe array 1 to probe array 3 is moderate. Our estimation proves that the line connecting these two probe arrays is nearly parallel to the magnetic field lines at the flux surface where the probes are located (especially for shot 4044). The correlation length of drift wave turbulence along the latter is long. Therefore, the coherencies in the AT frequency region are not very low for this set of data. In order to further verify this idea, the coherencies between E_{r2} and E_{r3} are examined and the results are given in Figs. 4(c) and 4(d). Here the coherencies of the GAMFZs are 0.79 and 0.69, respectively. The calculated toroidal wave vectors in the GAMZF frequency region are $k_\phi \simeq (0.1 \pm 0.2) \times 10^{-2}$ and $(0.4 \pm 0.1) \times 10^{-2}$ cm^{-1}, corresponding to toroidal mode numbers $n = 0.2 \pm 0.3 \simeq 0$ and $0.7 \pm 0.2 \simeq 1$. The important fact is that the coherencies are lower than 0.2 and no clear dispersion relations are observed for the ATs of this set of data. The physics reason is that the direction connecting probe arrays 2 and 3 is deviated from the magnetic field lines at the flux surface, and the correlation length of the ATs in this direction is much shorter than the distance between the two probe arrays. The similarity and the sharp contrast of the coherencies and the phase shifts between these two data sets in the GAM and turbulence frequency regions confirm that the observed oscillations of the GAM frequency are zonal flows of toroidal mode number $n \simeq 0$, while those of higher frequencies are turbulence of flute-type ($k_\parallel \simeq 0$) instabilities.

The three step structure of the LPs allows the radial characteristics of the potential perturbations to be easily determined. The radial component of the wave vector k_r calculated from ϕ_{f1} and $(\phi_{f2} + \phi_{f3})/2$ is presented in Fig. 5(a). The standard dispersion relations for the ATs and significant increases of k_r in the GAMZF frequency region indicate a very localized structure of the flows. With the contribution from the short wavelength ATs being filtered out, the more accurate radial wave vectors at the peak frequencies were calculated from ϕ_{f1} and ϕ_{f7} as $k_r = 1.5 \pm 0.2$ and 2.6 ± 0.2 cm^{-1} for the two shots.

To explore the generation mechanism of the GAMZFs, the squared cross-bicoherence [23,24] $\hat{b}^2(f_3) = |B(f_3)|^2/[\langle|v_r(f_1)v_\theta(f_2)|^2\rangle\langle|\phi_{f3}(f_3)|^2\rangle]$ of the perturbations is calculated. This is an indicator for the strength of nonlinear three wave coupling. Here the bispectrum $B(f_3) = \langle v_r(f_1)v_\theta(f_2)\phi^*_{f3}(f_3 = f_1 + f_2)\rangle$, with $v_r = (\phi_{f3} - \phi_{f2})/Bd_\theta$ and $v_\theta = E_{r1}/B$, while $\langle\cdots\rangle$ denotes an ensemble average and the number of realizations is $N = 200$. Figure 5(b) shows $b^2(f_3)$ plotted in the region between the lines of $f_1 = f_2$ and $f_1 = -f_2$ of the $f_1 - f_2$ plane for shot 4206. Positive and negative f_2 represent $f_3 = f_1 + |f_2|$ and $f_3 = f_1 - |f_2|$, respectively. The values of $b^2(f_3)$ about $f_3 = f_1 - |f_2| \simeq 7$ kHz and $f_2 \simeq \pm 7$ kHz are higher than the rest, indicating that the nonlinear three wave coupling is a plausible creating mechanism for the GAMZFs. The frequency resolution is 1 kHz in this analysis, and signals are significantly above the noise level of 0.005 in the wide range of frequency.

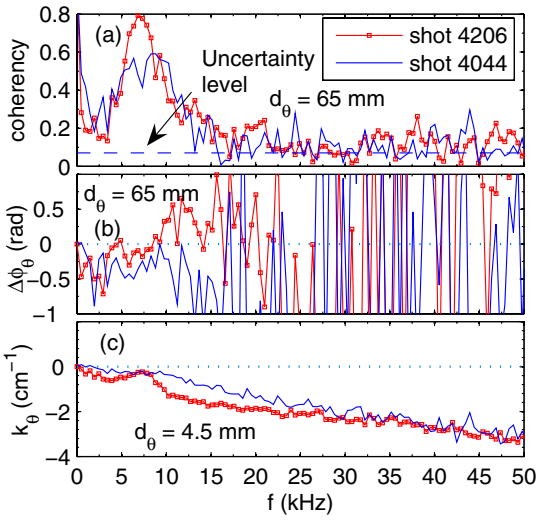

FIG. 3 (color online). (a) Poloidal coherency spectra of E_{r1} and E_{r2}, (b) the phase differences $\Delta\phi_\theta$ between E_{r1} and E_{r2}, and (c) the poloidal wave vector k_θ versus frequency f.

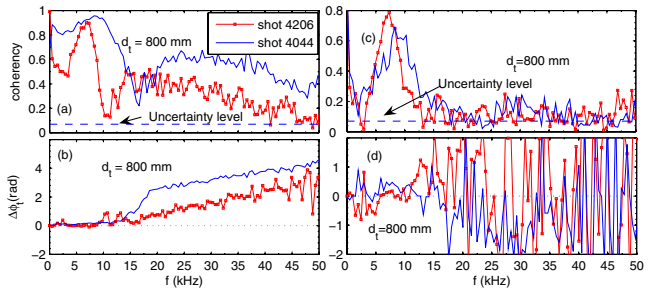

FIG. 4 (color online). (a) Toroidal coherency spectra of E_{r1} and E_{r3}, (b) phase differences $\Delta\phi_t$ between E_{r1} and E_{r3}, (c) toroidal coherency spectra of E_{r2} and E_{r3}, and (d) phase differences $\Delta\phi_t$ between E_{r2} and E_{r3}.

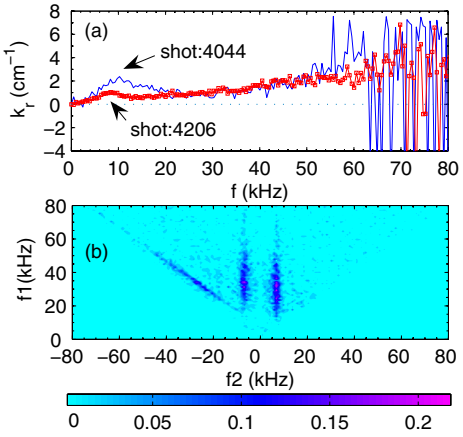

FIG. 5 (color online). (a) Radial wave vector k_r versus frequency f and (b) squared cross-bicoherence plotted in the $f_1 - f_2$ plane for shot 4206.

The zonal flow velocity is estimated as $v_{\theta ZF} \simeq 0.25$–$0.26$ km/s, while the measured amplitudes of the floating potential and the radial zonal electric field are 11–12 V and 0.60–0.62 kV/m, respectively. The shearing rate of the ZF [25] may be estimated as $\gamma_{sh} = k_r v_{\theta ZF} \sim 4$–$7 \times 10^4$/s, which is lower than but comparable with typical growth rate of drift instabilities of $\gamma_{dr} \sim \omega_{*e} \sim 10^5$/s for $L_n \sim 2$ cm and the decorrelation rate of the ATs $\sim 1/\tau_d = 10^5$/s. This is consistent with the above observations that a significant AT level is maintained in the experiments due to not high enough suppression effect of the ZF on the AT.

The spatial calibration accuracy for the LP radial positions is about 1 mm in the experiment. That could provide a finite wave vector component in the direction connecting the two poloidal LPs, $k \simeq k_r/65$ from a finite radial wave vector when the poloidal wave vector is zero. With the above k_r values of the GAMZFs, we got $k \simeq 0.023$ and 0.040 cm^{-1}, respectively, for the two shots. These are very close to the k_θ values given above. Therefore, the deviation of the measured poloidal feature of the GAMZFs from the theoretically predicted $m = 0$ symmetry may be attributed to the small radial offset between the poloidal measurements.

On the other hand, the mode numbers may be obtained from the linear equations $\mathbf{k} \cdot \boldsymbol{l}_i = \Delta\phi_{ti}$, with $\mathbf{k}$ and $\boldsymbol{l}_i$ ($i = 1, 2$) being the wave vector of the GAMZF and the displacement from the LP array i to array 3, respectively, while the $\Delta\phi_{ti}$ is the corresponding phase shift given in Fig. 4. The solutions we got for n are the average of the values given above. However, the solutions of $m = 0.36 \simeq 0$ and $0.80 \simeq 1$ are much lower than that estimated from Fig. 3 due to the possible cancellation of the contributions from finite k_r discussed above.

In summary, the three-dimensional features of the GAMZFs are identified simultaneously in the HL-2A tokamak experiments. In particular, the measurements of the toroidal symmetry of the GAMZF ($n \simeq 0$) in plasmas of a tokamak are the first of their kind and provide a crucial element linking experimental measurements to the theoretical predictions of the GAMZF axisymmetry structure. The other GAMZF features, such as poloidal symmetry, finite but narrow radial structure, and the nonlinear coupling mechanism for its creation, that have been observed previously are also identified comprehensively in conjunction with the unambiguous demonstration of the $n = 0$ symmetry. In addition, the high and low coherences of the higher frequency turbulence along and deviating from a magnetic field line, separating 80 cm in the toroidal direction, indicate that the turbulence has a flute-type instability characteristic.

The suggestions of K. Itoh, A. Fujisawa, and H. Sanuki are gratefully acknowledged. The authors thank the HL-2A Team for operation of the machine and J. Q. Li for helpful comments. This work is partly supported by the National Natural Science Foundation of China, Grants No. 10135020, No. 10235010, No. 10575031, No. 10335060, and No. 10375020.

[1] A. Hasegawa and M. Wakatani, Phys. Rev. Lett. **59**, 1581 (1987).
[2] Z. Lin *et al.*, Science **281**, 1835 (1998).
[3] F. L. Hinton and M. N. Rsenbluth, Plasma Phys. Controlled Fusion **41**, A653 (1999).
[4] K. Itoh *et al.*, Plasma Phys. Controlled Fusion **47**, 451 (2005).
[5] P. H. Diamond *et al.*, Plasma Phys. Controlled Fusion **47**, R35 (2005).
[6] A. Fujisawa *et al.*, Phys. Rev. Lett. **93**, 165002 (2004).
[7] G. S. Xu *et al.*, Phys. Rev. Lett. **91**, 125001 (2003).
[8] R. A. Moyer *et al.*, Phys. Rev. Lett. **87**, 135001 (2001).
[9] M. G. Shats *et al.*, Phys. Rev. Lett. **90**, 125002 (2003).
[10] N. Winsor *et al.*, Phys. Fluids **11**, 2448 (1968).
[11] P. M. Schech *et al.*, Rev. Sci. Instrum. **74**, 1846 (2003).
[12] M. Jakubowski *et al.*, Phys. Rev. Lett. **89**, 265003 (2002).
[13] G. R. McKee *et al.*, Phys. Plasmas **10**, 1712 (2003).
[14] G. R. McKee *et al.*, Plasma Phys. Controlled Fusion **45**, A477 (2003).
[15] G. R. Mckee *et al.*, Plasma Phys. Controlled Fusion **48**, S123 (2006).
[16] Y. Hamada *et al.*, Nucl. Fusion **45**, 81 (2005).
[17] Y. Nagashima *et al.*, Phys. Rev. Lett. **95**, 095002 (2005).
[18] G. D. Conway *et al.*, Plasma Phys. Controlled Fusion **47**, 1165 (2005).
[19] T. Ido *et al.*, Plasma Phys. Controlled Fusion **48**, S41 (2006).
[20] V. A. Vershkov *et al.*, Nucl. Fusion **45**, S203 (2005).
[21] A. V. Melnikov *et al.*, Plasma Phys. Controlled Fusion **48**, S87 (2006).
[22] Y. Liu *et al.*, Nucl. Fusion **45**, S239 (2005).
[23] P. H. Diamond *et al.*, Phys. Rev. Lett. **84**, 4842 (2000).
[24] Y. C. Kim *et al.*, IEEE Trans. Plasma Sci. **7**, 120 (1979).
[25] T. S. Hahm and K. H. Burrell, Phys. Plasmas **2**, 1648 (1995).